Journal of Mathematical Chemistry 4(1990)383–394

A HARMONIC OSCILLATOR MODEL OF THE CONFORMATIONALLY FLEXIBLE HELICAL POLYMERIC MOLECULES

Jerry A. DARSEY*
Department of Physical Sciences, Tarleton State University, Stephenville, TX 76402, USA
and
Wayne L. MATTICE
Department of Polymer Science, The University of Akron, Akron, OH 44325, USA

Abstract

The approach of the persistence vector to its asymptotic limit can be characterized by the average projection of a unit vector along the last bond onto a unit vector along the first bond. The behavior of this projection has been examined in simple, predominantly helical chains in which limited flexibility is introduced by either of two devices: occurrence in an average way of a configuration much different from that required for helix propagation, and use of a square-well potential centered at the dihedral angle utilized in a rigid helix. The manner in which flexibility is introduced determines the behavior of the angular frequency as well as the relative decay rates for oscillations and the midpoint about which oscillations occur.

1. Introduction

The end-to-end vector is an easily calculated configuration-dependent property of a chain molecule [1,2]. Averages of the components, when expressed in a coordinate system affixed to the first bonds in a chain [1], define a persistence vector $\boldsymbol{a}_n$. The X component can be related to the persistence length of the Porod–Kratky wormlike chain [3–5]. Particularly interesting examples of $\boldsymbol{a}_n$ are provided by flexible chain molecules in which short-range interactions tend to propagate a helical conformation. In such chains, $\boldsymbol{a}_n$ may oscillate as it approaches $\boldsymbol{a}_\infty$. The average projection of a unit vector along the last bond onto a unit vector along the first bond, denoted $\langle A_{xx} \rangle$, provides a simple characterization of the approach of $\boldsymbol{a}_n$ to $\boldsymbol{a}_\infty$. Brant and Burton [7] found that $\langle A_{xx} \rangle$ for amylose and dextrose chains oscillates at small n. Oscillations diminish, and eventually disappear, as n approaches large values.

The concern here is with two aspects of $\langle A_{xx} \rangle$ in simple, predominantly helical molecules. The point of departure is a simple chain in which all bond angles are 112° and all internal dihedral angles are 120° (in the convention where 0° denotes a *trans* placement). The chain is then a rigid *gauche* helix, and $\langle A_{xx} \rangle$ oscillates indefinitely as

*Permanent address: Department of Chemistry, The University of Arkansas at Little Rock, Little Rock, AR 72204, USA.

n increases. Flexibility is introduced by two procedures. *Trans* states occur in an average way in the first method. When the occupancy of a *trans* state is small, this procedure provides a simple model for a chain in which precisely helical segments are joined at bonds occupying a rotational state much different from the one required for helix propagation. The second method retains all bonds in the *gauche* state, but relaxes the definition of this state. Here, *gauche* states are distributed over the range $120° \pm \Delta\phi$. The perfect helix becomes continuously disordered as $\Delta\phi$ increases. Certain aspects of the behavior of $\langle A_{xx} \rangle$ are found to depend on the method by which flexibility is introduced.

2. Calculations

A right-handed coordinate system is affixed to each bond. The X axis runs along bond i from chain atom $i-1$ to chain atom i, and the Y axis is in the plane of bonds $i-1$ and i such that there is a positive projection of Y onto the X axis of the preceding bonds [1,2]. In establishing a coordinate system for the first bond, an imaginary zeroth bond is envisioned such that there is a *trans* placement about bond 1. Then we have

$$\langle A_{xx} \rangle = \text{row}(1, 0, 0) \langle T_1 T_2, \ldots, T_{n-1} \rangle \text{col}(1, 0, 0), \tag{1}$$

where statistical mechanical averages are enclosed in angular brackets and T_i denotes the transformation matrix for bond i. Simple chains dealt with here are considered to have bonds which are subject to the same rotational potential and behave independently, yielding

$$\langle A_{xx} \rangle = \text{row}(1, 0, 0) \langle T \rangle^{n-1} \text{col}(1, 0, 0). \tag{2}$$

With constant bond angle supplement θ, the average transformation matrix is

$$\langle T \rangle = \begin{bmatrix} \cos\theta & \sin\theta & 0 \\ \sin\theta\langle\cos\phi\rangle & -\cos\theta\langle\cos\phi\rangle & \langle\sin\phi\rangle \\ \sin\theta\langle\sin\phi\rangle & -\cos\theta\langle\sin\phi\rangle & -\langle\cos\phi\rangle \end{bmatrix}. \tag{3}$$

When flexibility is introduced by allowing the *a priori* probability for a *trans* placement at an internal bond to be p_t, the *trans* placements being distributed in an average way, then

$$\langle \cos\phi \rangle = p_t + (1 - p_t) \cos\phi_{g+}, \tag{4}$$

$$\langle \sin\phi \rangle = (1 - p_t) \sin\phi_{g+}, \tag{5}$$

where ϕ_{g+} is the dihedral angle for a *gauche* placement. When flexibility is introduced by allowing all ϕ in the range $\phi_{g+} \pm \Delta\phi$ to be equally probable, then

$$\langle \cos\phi \rangle = (2\Delta\phi)^{-1} \int \cos\phi \, d\phi, \tag{6}$$

$$\langle \sin\phi \rangle = (2\Delta\phi)^{-1} \int \sin\phi \, d\phi, \tag{7}$$

with integration limits being $\phi_{g+} \pm \Delta\phi$.

3. Results and discussion

3.1. SIGNIFICANCE OF CHAINS WITH $4j + 1$ BONDS

If *trans* placements were completely absent, $\langle A_{xx} \rangle$ would exhibit a pattern which propagates indefinitely as n becomes infinite. In contrast, when p_t is 0.0015, $\langle A_{xx} \rangle$ shows a general decay and, for n much larger than depicted in fig. 1(a), $\langle A_{xx} \rangle$ eventually approaches zero. Features reminiscent of a *gauche* helix are clearly recognized as this decay progresses. There is a tendency for a near repeat at every fourth bond, and there are also patterns of longer range, as shown by local minima (based on sequences of four bonds) for n of about 30 and 80.

The origin of the most interesting features becomes apparent when calculations are extended to much longer chains. The solid symbols in fig. 1(b) denote $\langle A_{xx} \rangle$ for chains containing $4j + 1$ bonds. These symbols pass through a minimum at $j = 26$ and attain a maximum when j is 52. The amplitude achieved at $j = 52$ is less than the amplitude of unity attained when j was zero. If fig. 1(b) were shaded to highlight chains containing $4j + 2$ bonds, the shaded symbols would pass through a maximum at $j = 12$ and a minimum at $j = 39$. The damped cosine nature of the curve would still be apparent. Chains with $4j + 3$ and $4j + 4$ bonds also have these features. Emphasis will be placed on chains having $4j + 1$ bonds. It should be noted that every chain having $4j + 1$ bonds would have $\langle A_{xx} \rangle = 1$ if bond angles were tetrahedral and all dihedral angles were 120°.

3.2. CHAINS CONTAINING *TRANS* PLACEMENTS

Figure 2 depicts $\langle A_{xx} \rangle$ for longer chains in which n is $4j + 1$. The amplitude decreases at successive local maxima when p_t is 0.0015. The consequences of an increase in p_t depend on the size of that increase. If p_t is doubled to 0.0030, the frequency is observed to decrease from that observed for $p_t = 0.0015$. It is also observed that for $p_t = 0.0030$, the decay of the amplitude toward zero is much greater.

The first objective is the description of heights and spacings (amplitude and frequency) of local maxima in fig. 2. A simple harmonic oscillator provides a successful model in the limit as p_t approaches zero.The equation is given by

$$m_1 \, d^2y/dt^2 + k_0 y = 0, \tag{8}$$

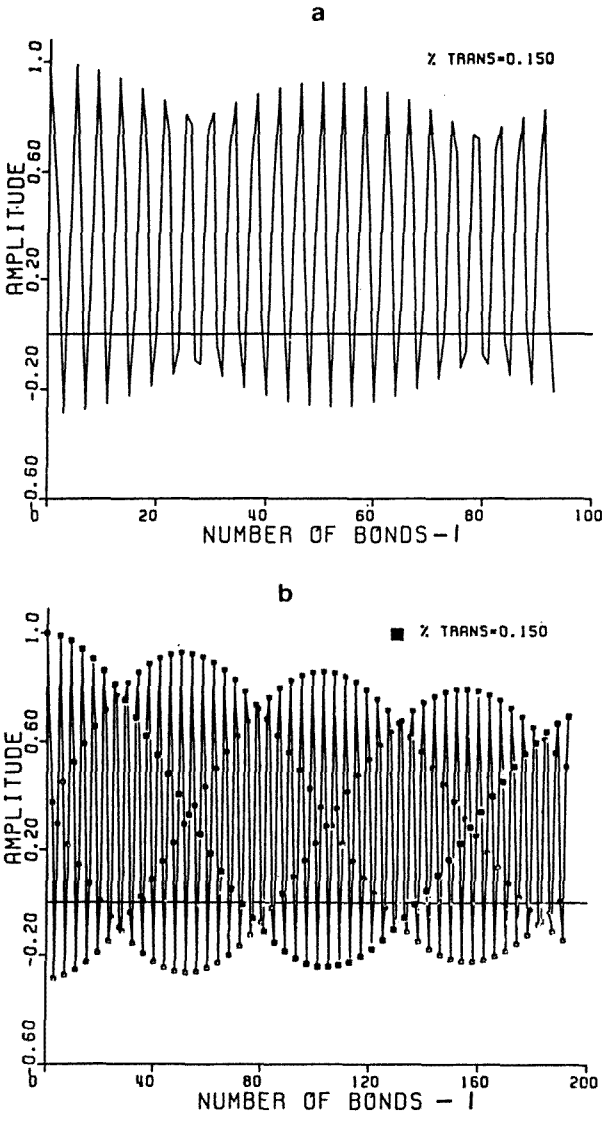

Fig. 1. (a) $\langle A_{xx} \rangle$ for chains with $\theta = 68°$, $\phi_{g+} = 120°$, and $p_t = 0.0015$; (b) $\langle A_{xx} \rangle$ for chains with $\theta = 68°$, $\phi_{g+} = 120°$, and $p_t = 0.0015$. Filled squares denote chains containing $4j + 1$ bonds.

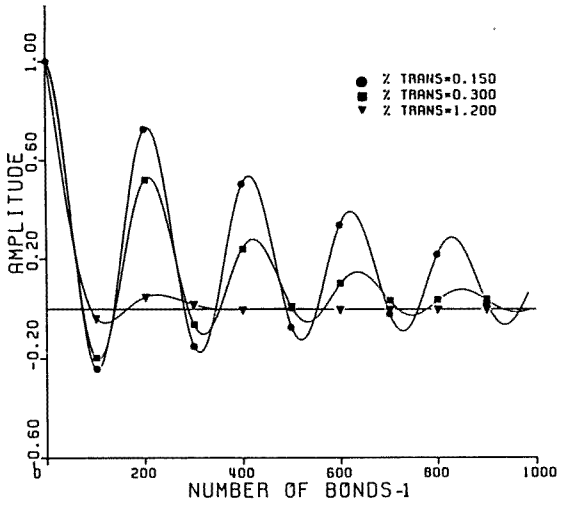

Fig. 2. $\langle A_{xx} \rangle$ for chains with $\theta = 68°$, $\phi_{g+} = 120°$, and the indicated percentage of *trans* placements for $4j + 1$ bonds.

with the solution given by

$$y = A \cos(\omega_0 t + \theta_0), \tag{9}$$

where A, m_1, k_0, t, y, ω_0, and θ_0 are, respectively, the maximum amplitude, mass, force constant, time, displacement, angular frequency, and initial phase constant. The angular frequency ω_0 is $(k_0/m_1)^{1/2}$. When p_t is zero, the behavior of local maxima for families of curves with $4j + i$ bonds is modeled with $A = 1$, $\theta = (i - 1)\pi/2$, and $\omega_0 t = 2\pi(n - 1)/n_{v,0}$ is the number of bonds per cycle.

Local maxima are described by a damped harmonic oscillator

$$d^2y/dt^2 + 2\gamma dy/dt + \omega_0^2 y = 0, \tag{10}$$

when p_t is small but nonzero. Here, γ is the damping coefficient. The oscillator is critically damped when $\gamma = \omega_0$, and the solution is given as

$$y = A \exp(-\gamma t)\,[\,y_0 + (v_0 + y_0)t], \tag{11}$$

where y_0 and v_0 are the initial displacement and velocity, respectively. The curve for $p_t = 0.0120$ in fig. 2 demonstrates an approach to critically damped behaviour.

The oscillator is underdamped when $\gamma < \omega_0$, and the solution then becomes

$$y = A \exp(-\gamma t) \cos(\omega_1 t + \theta_0), \tag{12}$$

where ω_1 is the angular frequency as given by

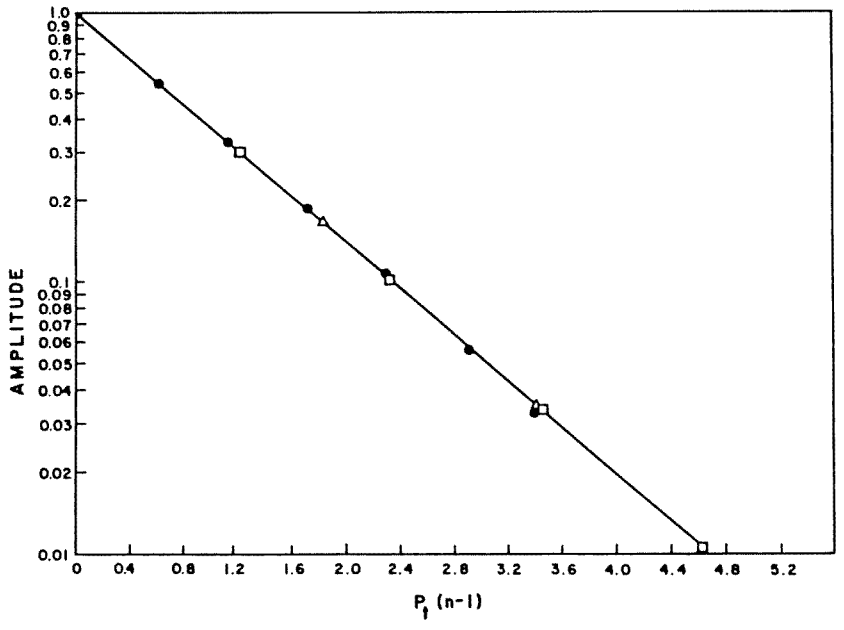

Fig. 3. $\langle A_{xx} \rangle$ at several local maxima as a function of $p_t(n-1)$. Circles, squares, and triangles denote the first, second, and third local maxima, respectively.

$$\omega_1^2 = \omega_0^2 - \gamma^2. \tag{13}$$

Figure 3 depicts $\ln\langle A_{xx} \rangle$ versus $p_t(n-1)$ at the first local maximum, for several p_t. Linearity is observed for p_t less than 0.012, but slight deviations from linearity occur at greater p_t. Also depicted in fig. 3 is $\ln\langle A_{xx} \rangle$ versus $p_t(n-1)$ for the second and third local maxima at several p_t. All points fall on the same line, as required by eq. (14) if this equation models correctly the heights of local maxima. Substituting into eq. (13) the values $k_1 p_t/2\pi$ for γ, $(1/n_v)^2$ for ω_1^2 and $(1/n_{v,0})^2$ for ω_0^2, we have the equation

$$(1/n_v)^2 = (1/n_{v,0})^2 - (k_1 p_t/2\pi)^2. \tag{14}$$

Equations (13) and (14) account for the frequency of oscillations. In order to account for all details of the features of fig. 2, recourse can be made to a damped harmonic oscillator viscously coupled to a second freely moving mass:

$$m_1 \mathrm{d}^2 y/\mathrm{d}t^2 = -ky - \lambda(\mathrm{d}y/\mathrm{d}t - \mathrm{d}y'/\mathrm{d}t), \tag{15}$$

$$m_2 \mathrm{d}^2 y'/\mathrm{d}t^2 = -\lambda(\mathrm{d}y'/\mathrm{d}t - \mathrm{d}y/\mathrm{d}t). \tag{16}$$

The viscous coupling constant is denoted by λ. Solving these two equations simultaneously yields

$$d^3y/dt^3 + (\lambda/m_1)(1 + m_1/m_2)\, d^2y/dt^2 + (k/m_1)\, dy/dt + (\lambda k/m_1 m_2)y = 0. \quad (17)$$

A general form of a third-order homogeneous differential equation is

$$d^3y/dt^3 - (Z_1 + Z_2 + Z_3)d^2y/dt^2 + (Z_1Z_2 + Z_1Z_3 + Z_2Z_3)dy/dt - Z_1Z_2Z_3\, y = 0, \quad (18)$$

where the solutions Z_i take the form

$$Z_{1,2} = -\gamma + i\omega, \quad (19)$$

$$Z_3 = -\alpha. \quad (20)$$

From eqs. (17)–(20), we obtain

$$\lambda m_1(1 + m_1/m_2) = 2\gamma + \alpha, \quad (21)$$

$$k/m_1 = 2\alpha\gamma + \gamma^2 + \omega^2, \quad (22)$$

$$\lambda k/m_1 m_2 = \alpha(\gamma^2 + \omega^2). \quad (23)$$

The most general form of the solution to eq. (17) is

$$y(t) = C_1 \exp(Z_1 t) + C_2 \exp(Z_2 t) + C_3 \exp(Z_3 t), \quad (24)$$

which, with eqs. (19) and (20) and Euler formulae, becomes

$$y(t) = A \exp(-\gamma t)\cos(\omega t + \theta) + B \exp(-\alpha t), \quad (25)$$

where A, B and θ are constants determined by initial conditions and γ, α, and ω are three independent parameters definable through eqs. (21)–(23). Making substitutions identical to those made to obtain eq. (14), together with the substitution $\alpha = k_2 p_t$, eq. (25) can be written as

$$\langle A_{xx} \rangle = A \exp[-k_1 p_t(n-1)] \cos[2\pi(n-1)/n_v + \theta] + (1 - A) \exp[-k_2 p_t(n-1)]. \quad (26)$$

The constants k_1 and k_2 can be determined with the aid of fig. 4. The distance from line C of fig. 4 (the midpoint about which oscillation occurs) to line A of this figure is depicted as line D in fig. 5. Performing a similar procedure for $p_t = 0.0010$, 0.0015, 0.0020, and 0.0040 leads to lines A, B, C, and E, respectively in fig. 5. The slopes of

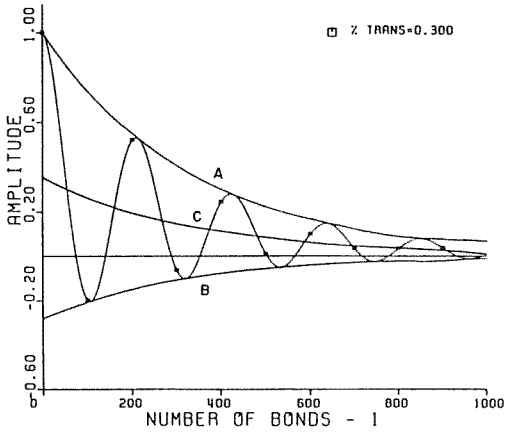

Fig. 4. $\langle A_{xx} \rangle$ for chains with $\theta = 68°$, $\phi_{g+} = 120°$, and $p_t = 0.0030$. Curves A and B connect local maxima and minima, respectively, for chains containing $4j + 1$ bonds. Curve C is drawn midway between A and B.

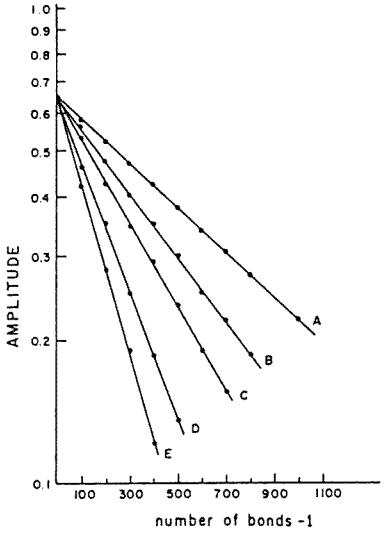

Fig. 5. Distance from line C to line A in plots of the kind depicted in fig. 4 when p_t has the following values: (A) 0.0010; (B) 0.0015; (C) 0.0020; (D) 0.0030; (E) 0.0040.

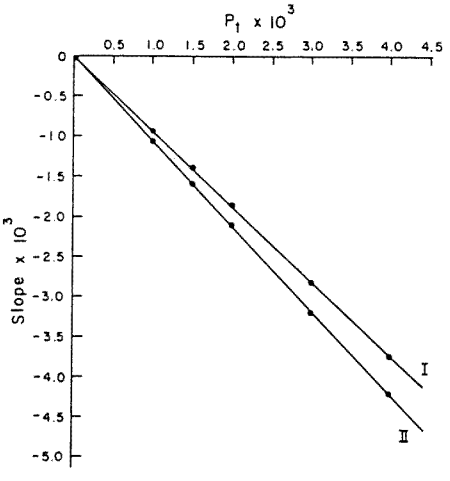

Fig. 6. Dependence upon p_t of the slopes of lines in (I) fig. 5; (II) fig. 7.

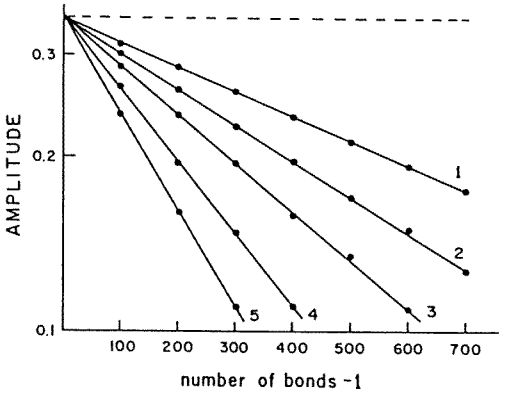

Fig. 7. Amplitude at line C in plots of the kind depicted in fig. 4 when p_t has the following values: (1) 0.0020; (2) 0.0015; (3) 0.0020; (4) 0.0030; (5) 0.0040.

these lines are depicted, as a function of p_t, as line I of fig. 6. The slope of line I is $-k_1$, as can be seen from eq. (26). The amplitude of curve C of fig. 4 is plotted as a function of $n-1$ in line 4 of fig. 7. Lines 1, 2, 3, and 5 of fig. 7 are generated in a like manner for values of $p_t = 0.0010$, 0.0015, 0.0020, and 0.0040, respectively. The slopes of these lines are shown as functions of p_t by line II of fig. 6. The slope of line II is $-k_2$. For a bond angle of 112°, $\phi_t = 0°$, and $\phi_{g+} = 120°$, k_1 and k_2 are 0.955 and 1.045, respectively. The nonequality of k_1 and k_2 signifies different decay rates for oscillations and the midpoint about which oscillations occur. The constant A in eq. (26) is found to be 0.655 from the intercept in either fig. 5 or fig. 7.

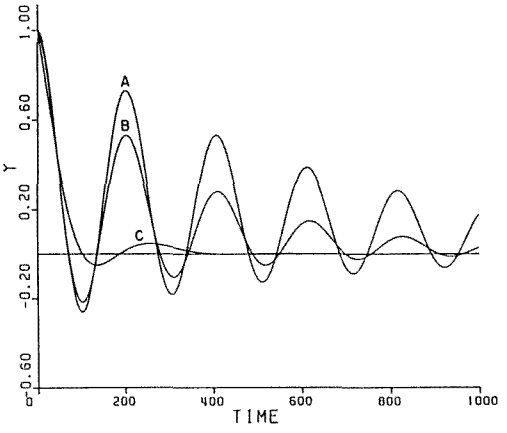

Fig. 8. $y(t)$ as a function of t from the solution of the damped harmonic oscillator viscously coupled to a second freely moving mass.

Figure 8 depicts the behavior of eq. (26) for $p_t = 0.0010$, 0.0030, and 0.0120 for A, B, and C, respectively. It can be seen that, using the parameters calculated previously, a plot of eq. (26) and a plot of $\langle A_{xx} \rangle$ of fig. 2 are totally superimposible, and calculations of random points on both plots show agreement to within the accuracy of single precision on an IBM 370/3033 computer. This would indicate that the differential equations (15) and (16) and the corresponding solution, eq. (26), successfully model the conformation of helical polymer molecules (which are found very commonly in proteins, DNA, RNA, etc.) with some built-in flexibility. It should be noted that the ratio k/m_1 can be calculated from eq. (22) using α, γ, and the frequency specified by fig. 2. The ratios λ/m_1 and m_1/m_2 can then be obtained via eqs. (21) and (23). Results are summarized in table 1. As expected, with increasing flexibility, the effective "drag mass", force constant, and viscous coupling constant all increase relative to m_1.

Table 1

Parameters deduced from the harmonic oscillator model

p_t	$\Delta\phi$ (deg)	α	γ	ω	k/m_1	λ/m_1	m_2/m_1
0.0015	0	0.0014	0.0016	0.0307	0.00104	0.0033	2.60
0.0030	0	0.0029	0.0032	0.0305	0.00114	0.0069	2.88
0.0120	0	0.0115	0.0126	0.0256	0.00146	0.0303	4.72
0	5	0.0008	0.0008	0.0308	0.00095	0.0016	2.00
0	10	0.0034	0.0033	0.0308	0.00098	0.0069	2.13
0	20	0.0135	0.0134	0.0308	0.00149	0.0302	2.98

3.3. CHAINS WITH SQUARE WELLS AT *GAUCHE* STATES

Figure 9 depicts $\langle A_{xx} \rangle$ for chains containing $4j + 1$ bonds when flexibility is introduced by having dihedral angles distributed in the range $120° \pm \Delta\phi$. Several similarities with fig. 2 can immediately be noted. A damped wave is evident and, for an increase in chain flexibility, there is a decrease in amplitude at a give local maximum.

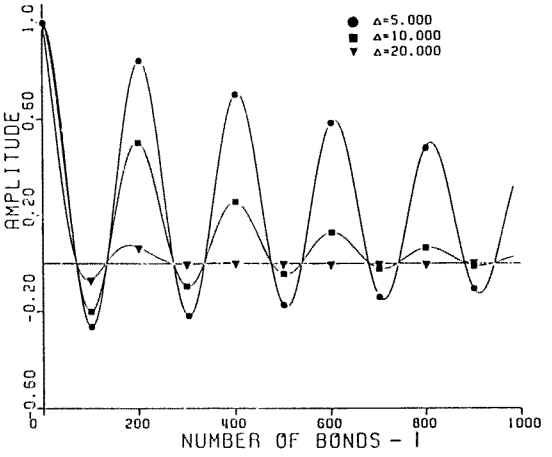

Fig. 9. $\langle A_{xx} \rangle$ for chains with $\theta = 68°$, $\phi_{g+} = 120°$, and the indicated $\Delta\phi$ for chains containing $4j + 1$ bonds.

Close inspection reveals that there are also differences in the behavior of $\langle A_{xx} \rangle$ in fig. 2 and fig. 9. This contrast is most readily apparent if attention is directed to the frequency of oscillations. In fig. 2, the frequency of the oscillations decreases (the spacing of local maxima increases) as p_t increases, but in fig. 9, the frequency is independent of $\Delta\phi$.

The behavior depicted in fig. 9 can be modeled by a damped harmonic coupled oscillator with a modification only to the values of α and γ of eq. (26). The connection

of local maxima and minima in fig. 9, as was done in fig. 4, and the construction of a figure similar to fig. 5, yields lines of different slopes. Extrapolation of these lines intersect the amplitude axis slightly below 0.655. Figure 10 depicts the manner in which slopes depend on $\Delta\phi$. The line through the points is calculated as a parabolic equation

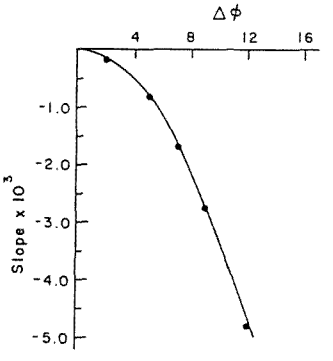

Fig. 10. Dependence upon $\Delta\phi$ of the slopes following the equation $(\Delta\phi)^2 = -9.04(\text{slope})$.

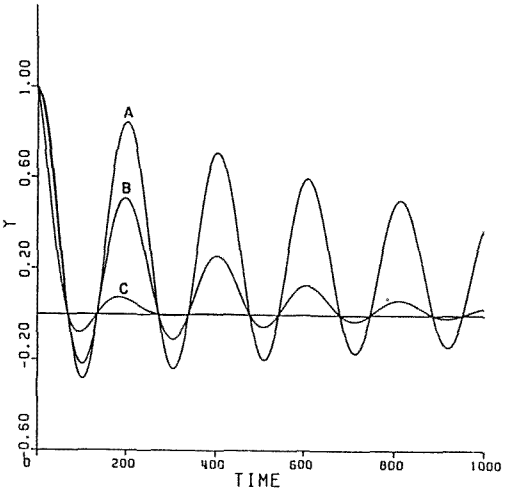

Fig. 11. $y(t)$ as a function of t, from the damped harmonic oscillator viscously coupled to a second freely moving mass as a model for chains in which flexibility arises from square-wells centered at *gauche* states. Curves A, B, and C correspond to $\Delta\phi$ values of 5°, 10°, and 20°, respectively.

$X^2 = P_1 Y$, where $X = \Delta\phi$, Y is the slope, and P_1 has the value -9.04. If another figure is constructed in the fashion of fig. 6, lines of differing slope are again obtained. A sum of unity is obtained for the intercept of these lines and the intercept in the figure described immediately above. When the slopes are plotted versus $\Delta\phi$, in the manner of fig. 10, a parabola is again obtained with a parameter P_2 being -9.12. P_1 and P_2 are analogous to k_1 and k_2 for our *trans* placement model. Both α and γ in eq. (18) are obtained by solving the appropriate parabolic equation for Y, with X corresponding to $\Delta\phi$. With the above substitutions, eq. (26) yields curves A, B, and C of fig. 11 for $\Delta\phi$ of 5°, 10°, and 20°. These curves are identical to those seen in fig. 9. In table 1, k/m_1, λ/m_1, and m_2/m_1 are collected, obtained using eqs. (21)–(23). All three ratios increase when the square-well becomes larger.

3.4. CONTRASTS IN BEHAVIOR OF THE TWO TYPES OF FLEXIBLE CHAINS

The angular frequency ω does not show any shift for the $\Delta\phi$ values cited in table 1. This result is in contrast to that seen when flexibility was produced by the introduction of *trans* placements. Of all parameters discussed here, ω is the most

sensitive to the manner in which flexibility is introduced into the helix. A second distinction lies in the behavior of α and γ. These two terms are nearly identical if flexibility is introduced by opening up the square-well. Under these circumstances, there are nearly identical decay rates for the midpoint about which oscillations occur and for the oscillations themselves. When flexibility is introduced via *trans* placements, γ is about 10% larger than α. Oscillations then decay somewhat more rapidly than does the midpoint about which oscillation occurs.

Can anything be said in general about the eigenvalues of $\langle T \rangle$? If λ_1 denotes the largest eigenvalue of $\langle T \rangle$, then since $\mathrm{row}(1,0,0)\,\langle T \rangle^{n-1}\mathrm{col}(1,0,0)$ approaches zero for a flexible chain as n approaches ∞, we assume that $-1 < \lambda_1 < 1$. If we have $0 < \lambda_1 < 1$, then λ_1^n must decrease monotonically as n increases. Hence, λ_1^n could not account for the oscillations in $\langle A_{xx} \rangle$. If $-1 < \lambda_1 < 0$, $|\lambda_1^n|$ decreases monotonically as n increases, with $\lambda_1^n > 0$ if n is even, and $\lambda_1^n < 0$ if n is odd. If λ_1^n controls the oscillations in $\langle A_{xx} \rangle$, the sign of $\langle A_{xx} \rangle$ must oscillate accordingly. However, if the sign of $\langle A_{xx} \rangle$ oscillates in any fashion other than that described, then the oscillations must be produced by some other feature of $\langle A_{xx} \rangle$.

4. Summary

This work demonstrates how coupled harmonic oscillators can be used to model an average conformational topology of a flexible helical molecule. Perhaps the most useful is the square-well potential about a *gauche* conformation. It is the authors' contention that there may be connections between some of the parameters describing the harmonic oscillators and conformational properties of helical molecules. There may also be some significance for the situation where $\gamma = \omega_0$ for the critically damped oscillator in that there may be a conformational phase change at this condition. If we were considering proteins, this could be the point where denaturing occurs or, more precisely, where the helix-coil to random-coil transition takes place. This would certainly be worthy of future investigations, both experimentally and theoretically.

Acknowledgements

The authors would like to thank the donors of the Petroleum Research Fund, administered by the American Chemical Society (W.L.M.) and the Robert A. Welch Foundation (J.A.D.) for support of this research. We would also like to thank Professor Doug Klein of Texas A&M at Galveston for valuable suggestions concerning this work and future work in this area.

References

[1] P.J. Flory, Proc. Nat. Acad. Sci. USA 70(1973)1819.
[2] P.J. Flory, Macromolecules 7(1974)381.
[3] G. Porod, Monatsh. Chem. 80(1949)251.
[4] O. Kratky and G. Porod, Rec. Trav. Chim. 68(1949)1106.
[5] P.J. Flory, *Statistical Mechanics of Chain Molecules* (Interscience, New York, 1969).
[6] D.Y. Yoon and P.J. Flory, J. Polym. Sci., Polym. Phys. Ed. 14(1976)1425.
[7] D.A. Brant and B. Barton, ACS Symp. Ser. 150(1981)81.